Chapter 7

Delay Lines and Multi-phase Transducers

In previous chapters we have considered the analysis of interdigital transducers and multi-strip couplers, the essential components of many surface-wave devices, and the variety of propagation effects that can be of practical significance. Here, and in subsequent chapters, we are mainly concerned with the design and performance of practical devices, making use of the earlier analysis to deduce many of the important features.

The simplest form of surface-wave device is the elementary delay line shown in Figure 7.1, consisting essentially of two identical uniform transducers. The function of this device is to delay an applied input signal without appreciably distorting it. The delay, related directly to the transducer separation, is typically in the range 1 to 50 μsec. Section 7.1 discusses this device, and is mainly concerned with the practical performance of uniform transducers. It should be noted that much of this discussion is directly relevant to other types of device, since uniform transducers are widely used. In addition, many of the conclusions apply qualitatively to more complex transducers, including the apodised transducers often used in bandpass filters and chirp transducers used in chirp filters. It will be seen that a delay line cannot generally be electrically matched such that the insertion loss is minimised, because this gives an unacceptable triple-transit output signal due to the acoustic reflectivity of the transducers. There are several special techniques for overcoming this limitation, in particular the use of multi-phase unidirectional transducers which are considered in Section 7.2.

In this chapter, the transducer analysis makes use of the quasi-static results of Chapter 4. Thus, electrode interactions are neglected, and this is usually valid in practice as discussed in Section 4.2. The reader is reminded that electrode interactions cause a small reduction of the surface-wave velocity within a transducer, and this is not allowed for in the analysis (Section 4.4).

7.1. DELAY LINES

In this section we consider delay lines using uniform transducers, such as that shown in Figure 7.1. In order to minimise the distortion of the applied signal the device must

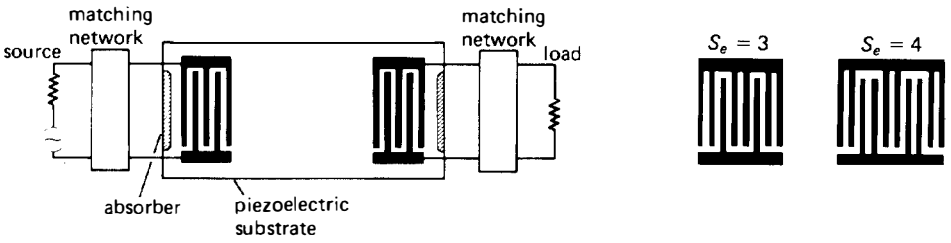

FIGURE 7.1. *Left*: Delay line using single-electrode transducers ($S_e = 2$). *Right*: Transducers with $S_e = 3$ or 4.

be non-dispersive, that is, its group delay must be almost constant over the band occupied by the signal spectrum. Chirp filters, which are very dispersive, are sometimes called dispersive delay lines, and are described in Chapter 9. We also exclude here non-dispersive delay lines using two chirp transducers, arranged such that the dispersion cancels.

Most of this section is concerned with the performance of transducers and their influence on the device performance, particularly on its bandwidth, insertion loss, and the level of the triple-transit output signal. These parameters can be found from the analysis of Chapter 4. The objective here is to illustrate some important practical features which arise when uniform transducers are used. For clarity some simplifying approximations are introduced, but the basic conclusions are nearly always valid in practice. Section 7.1.1 below considers the bandwidth and insertion loss of the device, including the effect of matching networks, and Section 7.1.2 discusses parasitics. The triple-transit signal is considered in Section 7.1.3, which also discusses methods of minimising it. Section 7.1.4 discusses the performance of practical delay lines, including special techniques of obtaining long delays or high frequencies.

7.1.1. Bandwidth and Conversion Loss of Uniform Transducers

Surface-wave devices often include simple matching networks, as indicated in Figure 7.1, to reduce the insertion loss. However, this is not always necessary, and sometimes it is advisable to omit the matching networks in order to minimise the triple-transit signal. Both cases will be considered here, and it will be seen that there is an interesting contrast in the role of the piezoelectric coupling parameter $\Delta v/v$. For unmatched transducers, $\Delta v/v$ has an important influence on the transducer conversion loss, which decreases as $\Delta v/v$ increases. When networks are included to reduce the loss, it is found that there is generally a trade-off between loss and bandwidth, and the trade-off is determined by the value of $\Delta v/v$. Thus the two cases have very significant practical differences.

We consider the common types of uniform transducer with $S_e = 2$, 3 or 4 electrodes per period, as illustrated in Figure 7.1. For the present, the matching networks will be excluded, so that each transducer in the device is connected directly to the source or load. For each transducer, an electrical equivalent circuit can be defined, such that its admittance equals the transducer admittance $Y_t(\omega)$. As shown in Figure 7.2(a), the circuit comprises a capacitance C_t, and acoustic conductance

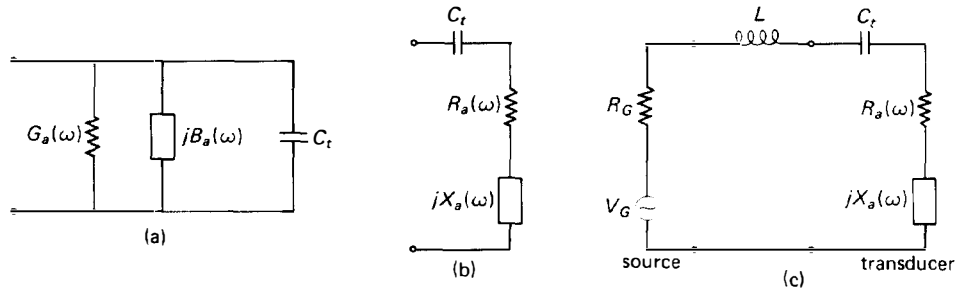

FIGURE 7.2. (a), (b): Equivalent circuits for transducer. (c): Tuned transducer connected to source.

$G_a(\omega)$ and susceptance $B_a(\omega)$, connected in parallel. Parasitic elements are ignored here, but will be considered in Section 7.1.2.

The fundamental centre frequency of the transducer is $\omega_c = 2\pi v_0/(pS_e)$, where p is the electrode pitch. For frequencies near ω_c, the conductance is, from equation (4.108),

$$G_a(\omega) \approx G_a(\omega_c)\left[\frac{\sin X}{X}\right]^2 \tag{7.1}$$

where $X = \pi N_p(\omega - \omega_c)/\omega_c$ and N_p is the number of periods. Thus $G_a(\omega)$ is maximised at $\omega = \omega_c$, as shown in Figure 4.14. The acoustic susceptance $B_a(\omega)$ is ignored here since it generally has little effect on the response (Section 4.6). When a generator is applied to the transducer, the power dissipated in the conductance accounts for the power of the generated surface waves. Assuming initially that the voltage across the transducer is independent of frequency, the surface-wave power is proportional to $G_a(\omega)$, and this gives the transducer bandwidth. Here we consider the 1.5 dB bandwidth, between the points where $G_a(\omega) = G_a(\omega_c)/\sqrt{2}$. since this is the 3 dB bandwidth of the delay line. From equation (7.1), the 1.5 dB transducer bandwidth $\Delta\omega$ is given by

$$\Delta\omega/\omega_c = 0.638/N_p. \tag{7.2}$$

This is called the *acoustic bandwidth*, since it does not allow for circuit effects.

The transducer Q-factor Q_t is, as in Section 4.6, given by

$$Q_t \equiv \frac{\omega_c C_t}{G_a(\omega_c)} = \frac{\tilde{Q}_t}{N_p \Delta v/v}, \tag{7.3}$$

where $\tilde{Q}_t$ is a constant near unity, given in Table 4.1 and Figure 4.15; for a single-electrode transducer ($S_e = 2$) with metallisation ratio $a/p = \frac{1}{2}$, we have $1/\tilde{Q}_t = 2.871$. Note that the acoustic bandwidth is not determined by Q_t, which refers to the equivalent electrical circuit.

For many transducers $N_p\Delta v/v \ll 1$, so that $Q_t \gg 1$, and this is assumed to be true here. For single-electrode transducers this condition is nearly always used, in order to

minimise electrode interaction effects. For $Q_t \gg 1$, equation (7.3) shows that the transducer admittance is dominated by the capacitive term $j\omega C_t$. Thus, quite large losses are generally incurred if the transducer is connected directly to a resistive source or load. The power conversion coefficient is given by equation (4.77).

Lower loss can be obtained by using an inductor to tune out the capacitance at frequency ω_c. If the inductor is connected across the transducer, the impedance seen by the source, at frequency is ω_c, is $1/G_a(\omega_c)$. For most transducers this is not close to 50 Ω, the usual source impedance. It is however often found that a good match can be obtained using a series inductor, and to appreciate this we consider an alternative equivalent circuit.

Series Equivalent Circuit and Matching. With an appropriate choice of component values, the transducer can be represented by the series equivalent circuit of Figure 7.2(b). It is convenient to include the transducer capacitance C_t explicitly, since this is usually the dominant term. The remaining components are the *radiation resistance* $R_a(\omega)$ and an acoustic reactance $X_a(\omega)$. When a voltage is applied to the transducer, the power dissipated in $R_a(\omega)$ accounts for the surface-wave power generated. Since the series and parallel circuits are equivalent, $R_a(\omega)$ and $X_a(\omega)$ can be found by equating the impedances of the two circuits of Figures 7.2(a) and (b). The reactance $X_a(\omega)$ generally has a form similar to $B_a(\omega)$, and is small at the centre frequency. The radiation resistance is found to be

$$R_a(\omega) = \frac{G_a(\omega)}{[G_a(\omega)]^2 + [B_a(\omega) + \omega C_t]^2}. \tag{7.4}$$

Since we assume $Q_t \gg 1$, the $G_a(\omega)$ and $B_a(\omega)$ terms in the denominator are insignificant, so that $R_a(\omega)$ is approximately proportional to $G_a(\omega)$, given by equation (7.1). Also, at the centre frequency, $R_a(\omega_c)$ is approximately equal to $G_a(\omega_c)/(\omega_c C_t)^2$. It is convenient to denote this quantity by $\hat{R}_a$, so that

$$R_a(\omega_c) \approx \hat{R}_a, \quad \text{for } N_p \frac{\Delta v}{v} \ll 1$$

and

$$\hat{R}_a \equiv G_a(\omega_c)/(\omega_c C_t)^2. \tag{7.5}$$

It was shown in Section 4.6 that $G_a(\omega_c)$ is proportional to $\omega_c N_p^2 W$, where W is the transducer aperture, and that C_t is proportional to WN_p. Thus $\hat{R}_a$ is proportional to $1/(\omega_t W)$, and is *independent* of the number of periods, N_p. It is also found that the aperture W can usually be chosen such that $\hat{R}_a$ is close to 50 Ω, and hence the transducer can be well matched to a 50 Ω source by means of a series inductor, as on Figure 7.2(c), where $L = 1/(\omega_c^2 C_t)$. When this is done, the centre-frequency conversion loss is ideally 3 dB, and the insertion loss for a delay line using two matched transducers is 6 dB. The value of $\hat{R}_a$ is therefore of considerable practical utility, as first noted by Smith *et al.* [197]. Transducers are usually designed with metallisation ratio $a/p = \frac{1}{2}$ since this maximises the efficiency, as shown by Figure 4.15. For a given value of a/p, $\hat{R}_a$ depends only on the value of S_e, the aperture W expressed in wavelengths, and the material parameters $\Delta v/v$, v_0 and ε_p^T.

TABLE 7.1

Apertures for uniform transducers with $\hat{R}_a = 50\Omega$. Fundamental response, $a/p = \frac{1}{2}$

	W/λ_c	
S_e	Y, Z lithium niobate	ST, X quartz
2	111	42
3	65	25
4	60	23

Table 7.1 gives data for Y, Z lithium niobate and ST, X quartz. The entries are values of W/λ_c required to give $\hat{R}_a = 50\Omega$, where $\lambda_c = 2\pi v_0/\omega_c = pS_e$ is the wavelength at the centre frequency. The data are obtained from materials parameters given in Table 6.1 and the analysis of Section 4.6, equations (4.111) and (4.115), together with equation (7.5). Typical apertures required are thus in the range 25 to 100 wavelengths; these are convenient practically since they generally give little diffraction spreading and the physical size, typically a few mm, is convenient for fabrication.

In some cases the transducer cannot be designed such that $R_a(\omega_c)$ is close to 50Ω. However, it is still possible to match to a 50Ω source if two reactive components are used. As shown in Figure 7.3(a), we consider a complex load $Z_0 = R_0 + jX_0$ representing the transducer, with a reactance X_1 added in series and a further parallel reactance X_2. Generally, R_0, X_0, X_1 and X_2 will all be functions of frequency. For any specified frequency it is possible to choose X_1 and X_2 such that the impedance seen at the terminals on the left is equal to a specified real value R_G. Using conventional network analysis, the required values of X_1 and X_2 are given by

$$(X_0 + X_1)^2 = R_0(R_G - R_0) \tag{7.6}$$

and

$$X_2 = -R_0R_G/(X_0 + X_1). \tag{7.7}$$

Since the left side of equation (7.6) must be positive, this method is valid only if $R_0 \leqslant R_G$. If this is so, there are two solutions for X_1 and X_2. If X_1 is positive the required reactance can be obtained by using an inductor with $L = X_1/\omega$, while for negative X_1 a capacitor can be used, with $C = -1/(\omega X_1)$. The same remarks apply for X_2.

An alternative circuit, in which the first reactance X_1 is in parallel with the load, is shown in Figure 7.3(b). It is convenient here to define G_0 and B_0 such that $G_0 + jB_0 = 1/Z_0$. For a resistive impedance R_G at the terminals on the left, it is found that X_1 and X_2 are given by

$$(B_0 - 1/X_1)^2 = -G_0(G_0 - 1/R_G)$$

and

$$X_2 = (B_0 - 1/X_1)R_G/G_0. \tag{7.8}$$

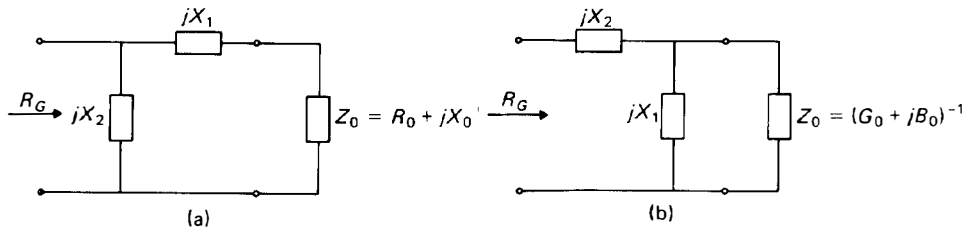

FIGURE 7.3. Two-component matching networks.

This method is valid if $G_0 \leqslant 1/R_G$. It is readily shown that at least one of the two circuits is valid for any specified values of Z_0 and R_G.

Bandwidth for Minimum loss. If the transducer is electrically matched to a source, at frequency ω_c, then all of the available power is converted into surface waves at this frequency. Thus the conversion loss is minimised, with a value of 3 dB due to the bidirectional nature of the transducer. One of the penalties paid for this low loss is that the matching circuit may substantially reduce the overall bandwidth, which is determined by the frequency variation of the surface-wave power generated. This circuit effect is significant when N_p is relatively small, and is associated with the electrical Q-factor of the circuit.

For the moment we consider only the series-tuned circuit of Figure 7.2(c), where the inductor tunes out the capacitance at frequency ω_c. Suppose first that N_p is small, so that the transducer acoustic bandwidth is large. In this case, for frequencies near ω_c, $R_a(\omega)$ can be taken as a constant approximately equal to $\hat{R}_a$, and $X_a(\omega)$ is small. Thus the circuit becomes a conventional series-tuned circuit. Since the transducer is matched we have $\hat{R}_a \approx R_G$, so that the Q-factor of the circuit is $1/(2\omega_c C_t \hat{R}_a)$. Using equation (7.5) we have $Q = \frac{1}{2}Q_t$, where Q_t is the transducer Q-factor of equation (7.3). We consider the bandwidth between the 1.5 dB points, where the power dissipated in the radiation resistance (that is, the surface-wave power) is equal to $1/\sqrt{2}$ times its maximum value. This is found to give a fractional bandwidth of $0.644/Q$, so that

$$\frac{\Delta\omega}{\omega_c} \approx \frac{1.29}{Q_t} = 1.29\frac{N_p\Delta v/v}{\hat{Q}_t}, \quad \text{for small } N_p. \tag{7.9}$$

For large N_p (but still subject to the constraint $N_p\Delta v/v \ll 1$), the transducer acoustic bandwidth is small, so that $R_a(\omega)$ varies rapidly with ω and the electrical bandwidth of the circuit is not relevant. In this case the bandwidth is approximately given by the transducer acoustic bandwidth of equation (7.2). There is however an additional complication arising because the transducer is matched to the source, and this will be considered further in Section 8.4.2 below. For a matched transducer, it is found that the 1.5 dB bandwidth is

$$\Delta\omega/\omega_c \approx 1.14/N_p, \quad \text{for large } N_p. \tag{7.10}$$

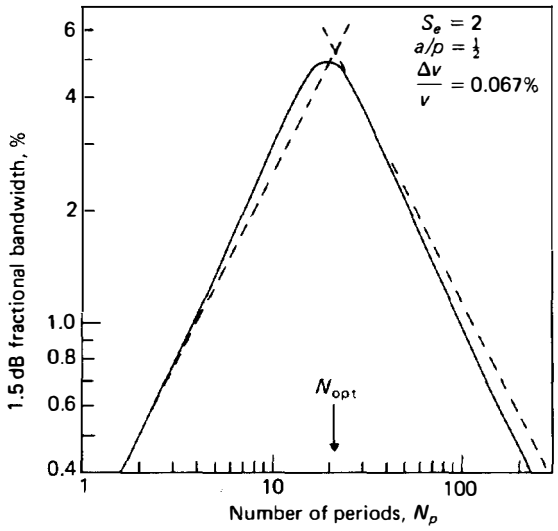

FIGURE 7.4 Bandwidth as a function of number of periods, for matched series-tuned single-electrode transducers on ST. X quartz.

Equations (7.9) and (7.10) are shown as broken lines on Figure 7.4, taking $\Delta v/v = 0.067\%$, appropriate for *ST*, *X* quartz. For equation (7.9), $\tilde{Q}_t$ is taken to be 1/2.871, appropriate for a single-electrode ($S_e = 2$) transducer with $a/p = \frac{1}{2}$. The bandwidth is proportional to N_p when N_p is small, and is proportional to $1/N_p$ when N_p is large. There is therefore an intermediate value of N_p at which the bandwidth is maximised, as first noted by Smith *et al.* [197]. The solid curve on Figure 7.4 is the 1.5 dB bandwidth calculated by analysing the circuit of Figure 7.2(c), using equation (7.1) for $G_a(\omega)$ and equation (4.110) for $B_a(\omega)$. The broken lines are seen to give a reasonable estimate for the bandwidth, for most values of N_p. The value of N_p for maximum bandwidth is denoted N_{opt}, and can be estimated by equating the bandwidths of equations (7.9) and (7.10), giving

$$N_{opt} \approx 0.55/\sqrt{\Delta v/v} \tag{7.11}$$

for $S_e = 2$ and $a/p = \frac{1}{2}$. Figure 7.4 also shows that the maximum bandwidth, obtained when $N_p \approx N_{opt}$ is given by $\Delta\omega/\omega_c \approx 1/N_{opt}$. Thus, for *ST*, *X* quartz ($\Delta v/v = 0.067\%$) we have $N_{opt} = 21$ and the maximum bandwidth is 4.8%. For *Y*, *Z* lithium niobate ($\Delta v/v = 2.15\%$), $N_{opt} = 4$ and the maximum bandwidth is 25%. Transducers with $S_e = 3$ or 4 give larger values of N_{opt}, and the maximum bandwidth is smaller, because $\tilde{Q}_t$ is larger (Table 4.1).

Trade-off Between Bandwidth and Loss. Clearly the overall bandwidth of a matched transducer cannot substantially exceed the electrical bandwidth or the acoustic bandwidth. If N_p is reduced, the acoustic bandwidth increases but the electrical bandwidth decreases. However, it is possible to increase the *electrical* bandwidth if the transducer does not need to be matched to the source. If the acoustic

bandwidth is also increased, by reducing N_p, this enables a larger overall bandwidth to be obtained, at the expense of larger conversion loss [198].

In the case of the series-tuned circuit of Figure 7.2(c), where now R_G is not necessarily equal to $\hat{R}_a$, the electrical Q of the circuit is $1/[\omega_c C_t(\hat{R}_a + R_G)]$, giving $Q = Q_t/(1 + R_G/\hat{R}_a)$. Thus a larger electrical bandwidth is obtained if $R_G > \hat{R}_a$. As before, the 1.5 dB electrical bandwidth is $0.644/Q$, and is therefore proportional to N_p, while the acoustic bandwidth, equation (7.2), is proportional to $1/N_p$. The optimum value of N_p can be estimated by equating the bandwidths. The centre-frequency conversion loss, obtained by analysing Figure 7.2(c), is given by

$$\text{conversion loss} \approx 10 \log [\tfrac{1}{2}(1 + \hat{R}_a/R_G)^2 R_G/\hat{R}_a] \quad \text{(dB)}, \tag{7.12}$$

which gives 3 dB when $R_G/\hat{R}_a = 1$, and greater losses for other values of $R_G/\hat{R}_a$. The maximum 1.5 dB bandwidth can therefore be evaluated as a function of conversion loss by increasing $R_G/\hat{R}_a$, and evaluating the optimum value of N_p for each value of $R_G/\hat{R}_a$. Figure 7.5 shows the result obtained by numerical analysis [199]. To a good approximation, a universal curve valid for all materials is obtained if the fractional bandwidth is divided by $\sqrt{\Delta v/v}$. The figure includes scales giving the required optimum value of N_p, for ST, X quartz and Y, Z lithium niobate. For conversion losses greater than about 7 dB, the optimum value of N_p is approximately $1/(2\Delta\omega/\omega_c)$.

The value of $R_G/\hat{R}_a$ can be increased by increasing the aperture W, since $\hat{R}_a$ is proportional to $1/W$. However, a sufficient increase cannot always be conveniently

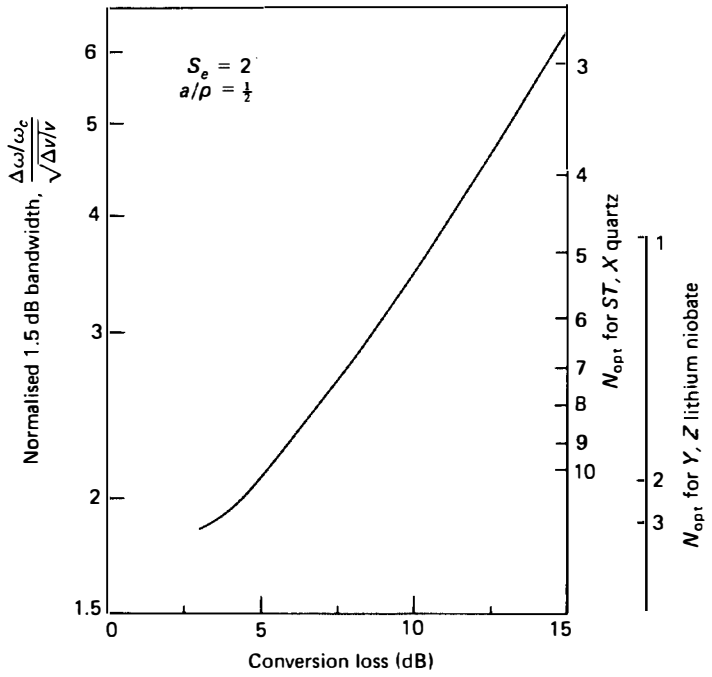

FIGURE 7.5. Maximum bandwidth as a function of conversion loss, for series tuned single-electrode transducers.

obtained by this method. An alternative method is to use a transformer, so that the transducer "sees" a source impedance greater than 50Ω. The two-component circuits of Figure 7.3 can be used for this purpose, though since they only act as ideal transformers at one frequency the above discussion is not strictly valid for this case. Reeder *et al.* [200] have developed this method using an inverter network, essentially a cascade of several two-component sections of the type shown in Figure 7.3. Using $N_p = 1$ in each transducer, they demonstrated a *Y*, *Z* lithium niobate delay line with a 3 dB bandwidth of 43%, centred at 105 MHz, and with 15 dB insertion loss.

A related problem is that of efficient matching into a series resonant circuit, given that some specified bandwidth is required. Reeder and Sperry [201] have investigated the use of a transmission line to give the required impedance transformation for this case.

An alternative method of obtaining wide fractional bandwidths is to use chirp transducers (Chapter 9), arranged such that the dispersion cancels. This is sometimes preferable as it gives transducer designs less sensitive to strays.

Standing-wave Ratio. In some applications the reflection of the electrical signal applied to the device is of some concern, since this causes standing-wave effects if the device is used with cables of length comparable with the electromagnetic wavelength. The requirement is usually specified in terms of the voltage standing wave ratio (VSWR), equal to $(1 + R)/(1 - R)$, where R is the magnitude of the voltage reflection coefficient. If there are no resistive losses in the transducer or matching network, the transducer conversion loss is $-10 \log (1 - R^2)/2$ (dB), and is thus directly related to the VSWR. In practice this requirement can be very restrictive. For example, if the VSWR is not to exceed 2, as is often the case, the conversion loss must not exceed 3.5 dB, and therefore must not vary by more than 0.5 dB over the specified band. Thus the VSWR requirement can usually be met only over a small part of the transducer acoustic bandwidth.

Better VSWR performance can be obtained by adding a series resistor, since this enables an impedance close to the characteristic impedance of the cable to be obtained, without requiring the transducer itself to be closely matched. Smith [202] has discussed this method in detail, showing the relevant trade-offs. There is however the disadvantage that the additional resistor dissipates power, thus increasing the insertion loss of the device. An alternative solution is to incorporate well-matched amplifiers, with good reverse isolation, into the same package as the surface-wave device. This improves the VSWR without significantly degrading the overall noise figure.

7.1.2. Parasitic Components

In this chapter it has been assumed so far that any parasitic components, such as stray capacitance or the resistivity of the electrodes, have negligible effects on the transducer performance. This is often true for transducers operating at relatively low frequencies, but at high frequencies strays can be very significant. We consider first the electrode resistivity, a particularly important effect which can often be predicted fairly accurately.

(a) Electrode Resistivity. We assume here that the resistivity of the electrodes is small, and that it can be represented by adding a series resistance R_E to the ideal equivalent circuit, as shown in Figure 7.6(a). For the analysis here the transducer is taken to be unapodised and to have regular electrodes, though it is not necessary to constrain it to be uniform; thus the discussion here applies, for example, to the transducer of Figure 4.9(a), which was analysed in Section 4.5. To estimate the value of R_E it is assumed that piezoelectric coupling can be neglected, so that the transducer behaves as a capacitor with capacitance C_t.

We consider first the current in electrode n, when the resistivity is negligible. When unit voltage is applied across the transducer, the total charge on electrode n is q_n, given by equation (4.90), and the current entering the electrode is therefore $j\omega q_n$, at frequency ω. Since the charge density is uniform in the y-direction, along the length of the electrode, the current varies linearly in this direction. Thus the current at some point y is given by

$$I_n(y) = j\omega q_n(\tfrac{1}{2} \pm y/W), \tag{7.13}$$

where W is the transducer aperture and the origin for y is taken to be centrally located in the transducer. The sign in equation (7.13) depends on which bus-bar the electrode is connected to. The current is invariant across the width of the electrode.

A small amount of resistivity, such that $R_E \ll 1/(\omega C_t)$, has little effect on the voltage across the ideal transducer, or on the electrode currents given by equation (7.13). The main consequence is a loss of power, which can be accounted for by the resistance R_E. It is assumed that the bus-bars are wide enough for their resistance to be negligible. Defining r_E as the resistance of one electrode per unit length, the power dissipated in electrode n is

$$P^{(n)} = \tfrac{1}{2} r_E \int_{-W/2}^{W/2} |I_n(y)|^2 \, dy = r_E \omega^2 q_n^2 W/6. \tag{7.14}$$

The total power lost is the sum of the $P^{(n)}$, and is equated with the power dissipated in R_E. Since the current through R_E is approximately $j\omega C_t$, we have

$$\sum_{n=1}^{N} P^{(n)} = \tfrac{1}{2}\omega^2 C_t^2 R_E,$$

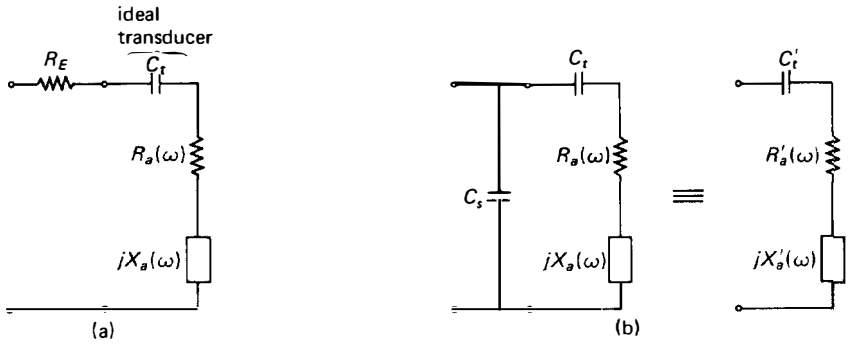

FIGURE 7.6. Representation of (a) electrode resistance, (b) stray capacitance.

where N is the number of electrodes. Using equation (4.91) for C_t, it is found that R_E is given by

$$R_E = \frac{r_E W}{3}\left[\sum_{n=1}^{N} q_n^2\right] \Big/ \left[\sum_{n=1}^{N} \hat{P}_n q_n\right]^2, \tag{7.15}$$

where $\hat{P}_n = 0$ or 1 is the polarity of electrode n. The values of the q_n are given by the analysis in Section 4.5.1.

For the uniform transducers of Figure 7.1 the relative values of the q_n can be readily reduced from symmetry arguments, assuming end effects to be negligible. We thus find

$$\begin{aligned} R_E &= 2r_E W/(3N_p), \quad \text{for } S_e = 2, \\ &= r_E W/(2N_p), \quad \text{for } S_e = 3, \\ &= r_E W/(3N_p), \quad \text{for } S_e = 4. \end{aligned} \tag{7.16}$$

The resistance of one electrode per unit length is $r_E = \varrho/a$, where a is the electrode width and ϱ is the resistivity of the metal film, in ohms per square. For the frequencies and film thicknesses of interest here the skin effect is insignificant and, except for very thin films, the resistivity is found to correspond quite well with the bulk resistivity of the metal. Measurements on aluminium films [203] give

$$\varrho \approx 0.04/h \quad \text{ohm/square} \tag{7.17}$$

for $h \geqslant 0.05$, where h is the film thickness in μm. For smaller values of h the resistivity increases more rapidly. Typical experimental film thicknesses are in the range 0.05 to 0.3 μm.

For practical transducer designs, R_E values of 20 Ω or greater are not unusual. The practical significance of this can be found by analysing the circuit of Figure 7.6(a), including the source and any matching network. It is often the case that the losses become significant when R_E is comparable to, or greater than, $\hat{R}_a$. Thus, it is generally important to consider the electrode resistivity when designing transducers. If the predicted value of R_E is too large it may be reduced by increasing h or by reducing the aperture W, since $R_E/\hat{R}_a$ is proportional to W^2.

A more detailed analysis of the effects of electrode resistivity has been given by Lakin [204] who showed that, in addition to the loss of power, there is a variation of voltage along the length of any one electrode. This implies that the power of the surface wave generated by the transducer will vary across its aperture. However, if the resistivity is small, Lakin's analysis shows that an external resistance R_E may be added, as above, to account for the power loss. Also, for $R_E \leqslant \hat{R}_a$ the voltage variations are usually insignificant. Thus the expressions given above generally give an adequate representation of electrode resistivity, for practical purposes.

(b) Other Parasitic Components. In many cases, stray capacitance between the transducer and the package can be significant. Thus, if R_E is negligible the transducer may be represented as in Figure 7.6(b), where a stray capacitance C_s is connected across the ideal transducer. It is convenient to consider the effect of this in

terms of an equivalent series circuit with components C_t', $R_a'(\omega)$ and $X_a'(\omega)$; these components can be evaluated by equating the impedances of the two circuits in Figure 7.6(b). For simplicity it is assumed that, as for most transducers, $R_a(\omega) \ll 1/(\omega C_t)$ and $X_a(\omega) \ll 1/(\omega C_t)$, and it is then found that

$$R_a'(\omega) \approx R_a(\omega) \frac{C_t^2}{(C_t + C_s)^2} \tag{7.18}$$

and

$$C_t' \approx C_t + C_s \tag{7.19}$$

Thus the stray capacitance causes an apparent reduction of the radiation resistance, affecting the matching, and an apparent increase of the transducer capacitance. These effects are usually of practical significance if C_s is in the region of $C_t/4$ or greater. In practice, C_s is typically $\frac{1}{2}$ to 1 pF, but transducer capacitances can sometimes be comparable with this, particularly for high-frequency operation.

Several other types of parasitic component can be significant, for example the resistance of tuning inductors, and stray capacitance associated with pins or connectors on the package. Resistance of the transducer bus-bars can be significant, though usually the bus-bar width can be made large enough for this resistance to be negligible. In long transducers the inductance of the bus-bars can be relevant, causing them to behave as a transmission line; this effect is discussed briefly in Section 9.5.4.

Slobodnik [205] has discussed in more detail the effects of stray components on device performance. It can be concluded that for high frequency devices, above about 300 MHz, a detailed assessment of the effects is needed as part of the design procedure, and considerable care is needed in package design. At lower frequencies, strays are generally less consequential.

7.1.3. Triple-transit Signal

In addition to the desired output signal, a surface-wave delay line also produces an unwanted triple-transit signal due to acoustic reflections, as discussed in Section 4.2. It is usually important to ensure that the triple-transit signal is adequately suppressed. Here we consider the triple-transit signal for a device with uniform transducers, and show that there is a trade-off between triple-transit suppression and insertion loss.

Considering the delay line of Figure 7.1, the transducers and matching networks are taken to be identical, and the load impedance is assumed to be equal to the source impedance. The reflection coefficients of the two transducers are therefore the same. As discussed in Section 4.8, the output voltage is the sum of the main signal V_1 and the triple-transit signal V_3. If the device input signal is C.W., with frequency ω, the magnitudes of these are in the ratio

$$|V_3/V_1| = |r(\omega)|^2, \tag{7.20}$$

where $r(\omega)$ is the amplitude reflection coefficient of each transducer. Propagation loss and diffraction are assumed to be negligible here. For an unapodised transducer with negligible electrode interactions we have, from equation (4.78),

$$|r(\omega)|^2 = \frac{G_a(\omega)}{2G_L} C(\omega), \tag{7.21}$$

where $C(\omega)$ is the power conversion coefficient, so that the conversion loss is $-10 \log [C(\omega)]$. Equation (7.21) is valid provided there are no strays and the matching network is purely reactive. The quantity G_L is the real part of the admittance $Y_L(\omega)$ "seen" by the transducer.

The transducers are taken to be uniform, and we consider the triple-transit signal at the centre frequency ω_c. Each transducer is assumed to be tuned with a series inductor, as in Figure 7.2(c), with $L = 1/(\omega_c^2 C_t)$. In this case G_L equals the real part of $(R_G + j\omega L)^{-1}$. Assuming that Q_t is large we have $\omega_c C_t \hat{R}_a \ll 1$ and $X_a(\omega_c)$ is negligible, and it is found that $G_a(\omega_c)/G_L \approx \hat{R}_a/R_G$. Equations (7.20) and (7.21) thus give

$$|V_3/V_1| = \tfrac{1}{2} C(\omega_c) \hat{R}_a/R_G. \tag{7.22}$$

For a launching transducer, the power conversion coefficient $C(\omega)$ is defined as the ratio of the surface-wave power generated (in one direction) to the power available from the source, and from Figure 7.2(c) we find

$$C(\omega_c) = \frac{2\hat{R}_a/R_G}{(1 + \hat{R}_a/R_G)^2}. \tag{7.23}$$

The insertion loss of the device is $-20 \log [C(\omega_c)]$, in dB. We define the *triple-transit suppression* as the power ratio, in dB, of the main and triple-transit signals, equal to $-20 \log |V_3/V_1|$. Both quantities are thus expressed as functions of the ratio $\hat{R}_a/R_G$, so the triple-transit suppression can be plotted as a function of insertion loss. This is shown as the solid curve in Figure 7.7. When $R_G = \hat{R}_a$ the transducers are matched

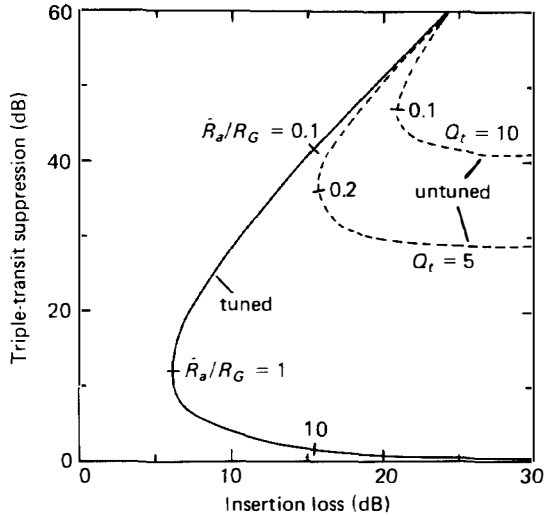

FIGURE 7.7. Triple-transit suppression for unapodised transducers.

and the triple-transit suppression is 12 dB. Better triple-transit suppression is obtained, at the expense of greater loss, by increasing $R_G/\hat{R}_a$. For large values of $R_G/\hat{R}_a$, the triple-transit suppression is equal to twice the insertion loss, plus 12 dB. In practice, the triple-transit suppression is often better than the predictions of Figure 7.7, due to the presence of strays and propagation loss.

The broken lines in Figure 7.7 refer to untuned transducers, that is, the same situation except that the inductors are omitted. The curves are obtained from equations (7.20) and (7.21), using circuit analysis to evaluate $C(\omega_c)$. In this case the trade-off between triple-transit and insertion loss depends on the transducer Q-factor, Q_t.

It should be noted that the above discussion refers to C.W. excitation of the device. If a rectangular pulse is applied, with carrier frequency ω_c, the device output gives a pulse due to the main response followed by a smaller pulse due to the triple-transit signal, and these are resolved if the transducer separation is sufficient. If the input pulse is long enough, so that its bandwidth is much less than the delay line bandwidth, the ratio of the output pulse powers gives the C.W. triple-transit suppression discussed above. For a short input pulse this is not so; to calculate the ratio of the output pulse amplitudes it is necessary to use the device frequency responses $H_1(\omega)$ and $H_3(\omega)$ of Section 4.8, allowing for the spectrum of the input pulse.

Reduction of Triple-transit Signal. Surface-wave devices are often required to give a triple-transit suppression of 40 dB or more, and Figure 7.7 shows that this requires the insertion loss to exceed 15 dB. Although this is often acceptable, there are many applications where good triple-transit suppression and low loss are required simultaneously. For this purpose, a number of special methods have been developed. Since the finite reflection coefficient of a matched transducer is associated with its bidirectional nature, one type of solution is to use a *unidirectional* transducer, designed such that it can generate surface waves in only one direction. If such a transducer is matched, the reflection coefficient for incident surface waves is, ideally, zero and the triple-transit signal vanishes. A type of undirectional transducer using a multi-strip coupler is considered in Section 5.4 above. There are also several types of *multi-phase* transducers that are unidirectional, and these are considered in Section 7.2 below. In addition to reducing the triple-transit signal, unidirectional transducers also give very low insertion loss, ideally 0 dB. However, these transducers are strictly unidirectional only at one frequency, so the triple-transit signal is not entirely eliminated.

Other methods of reducing the triple-transit signal are shown in Figure 7.8. In the *three-transducer scheme* [206] of Figure 7.8(a), the two outer transducers are connected in parallel. All three transducers are unapodised, and the entire structure is symmetrical about the centre line. Thus the central transducer is symmetrical, and the outer transducers have the same geometry as each other. The waves generated by the outer transducers arrive at the central transducer with equal amplitude and phase, and it is found that no reflected waves are produced if the central transducer is electrically matched. This is to be expected by reciprocity, since a symmetrical transducer generates waves of equal amplitude and phase when a voltage is applied

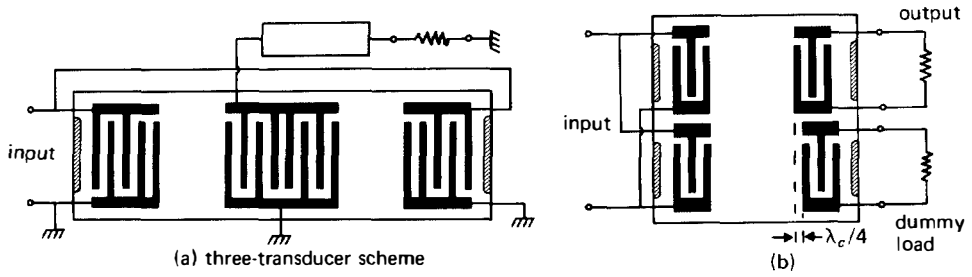

FIGURE 7.8. Methods of reducing triple-transit signals.

to it. The device may be analysed by the methods of Chapter 4. In particular, it can be shown from the scattering matrix of equation (4.79) that the central transducer does not reflect if it is matched; this follows because the symmetry implies that $\bar{\varrho}_e(k_0)$ is real. An additional advantage is that the central transducer converts all the incident surface-wave power into output power, so that the minimum insertion loss for the device is ideally 3 dB.

The three-transducer scheme is also effective if the central transducer is apodised, or if the outer transducers are apodised, provided the symmetry is preserved. In these cases, the triple-transit signal is eliminated if a suitable choice is made for the electrical admittance "seen" by the central transducer, though the admittance required does not match the transducer and so the insertion loss is not minimised. The required admittance can be deduced from the analysis of Chapter 4.

Another method, shown in Figure 7.8(b), essentially comprises two delay lines constructed on one substrate [206]. The transducers at one end are connected together, while those at the other end are connected separately to equal loads; one of the loads is the device output, while the other is a dummy. One of the output transducers is displaced relative to the other by an amount $\lambda_c/4$, where λ_c is the surface-wave wavelength at frequency ω_c. At this frequency, waves reflected by the output transducers are in anti-phase and so do not excite the input transducers; thus, no reflected waves reach the output transducers. However, this is true only at one frequency. In addition, because of the power dissipated in the dummy load the minimum insertion loss obtainable is 9 dB. There are however several variants of the method. Tanski and Van De Vaart [207] have shown that, if double-electrode transducers are used, the required phase relationship between the reflected waves can be obtained by modifying the transducer geometries instead of using a displacement. The triple-transit suppression obtained is then, in principle, independent of frequency. Gunton [208] has investigated several schemes in which the transducers at each end are connected to a hybrid coupler, showing that the loss due to the presence of the dummy load in Figure 7.8(b) can be eliminated. A related method is used in the multi-strip echo trap, mentioned in Section 5.5.

7.1.4. Delay Line Types and Performance

The simplest type of surface-wave delay line is the two-transducer device illustrated in Figure 7.1. The performance of this device has been discussed above, though

diffraction and propagation loss have not been considered. These effects can contribute significantly to the insertion loss, especially at high frequencies, and are discussed in Sections 6.2 and 6.3 above.

In some cases the device is required to have a series of outputs, giving different delays of the input signal. Such a device is called a *tapped* delay line, and is readily implemented by using a separate transducer for each output; in this case the output transducers are often called "taps". A closely related device is the PSK filter designed to correlate a phase-coded waveform, using a sequence of taps connected together. This is considered in Chapter 10.

Long Delay Techniques. As for other surface-wave devices, the maximum delay of the basic type of delay line is limited to about 50 μsec because of the lengths of available substrate materials. Several special techniques for obtaining longer delays have been investigated. The use of multi-strip track-changers has already been mentioned in Section 5.5. Another method is the *wrap-around* technique in which the ends of the substrate are rounded into smooth cylindrical surfaces, so that a surface wave can circulate around the substrate several times [209]. For example, a device using a bismuth germanium oxide substrate gave 908 μsec delay at 85 MHz centre frequency, with 65 MHz bandwidth and 65 dB insertion loss. A similar principle is used in the *disk delay line* [210], where the substrate is in the form of a circular disk; this exploits a subtle topographic effect in which the rounded edge acts rather like a surface-wave lens, limiting the diffraction spreading. However, neither the disk nor the wrap-around method has been widely used, owing to fabrication and mounting complications.

Another approach for long delays is *cascading*, in which several devices are connected in sequence, alternating with amplifiers to compensate for the device losses. In this case the amplitude response of each device needs to be exceptionally flat in order to obtain adequate fidelity for the overall system. For example, a tapped 400 MHz delay module including amplifiers gave 40 μsec delay, and had a response flat within $\pm$ 0.5 dB over a 100 MHz bandwidth [211]. Such modules can be cascaded to give delays of several hundred microseconds. Another example is an 800 MHz module giving 7.5 μsec delay, with a response flat to $\pm$ 0.2 dB over a 230 MHz bandwidth [212]. In both cases lithium niobate substrates were used.

Several special techniques have been used to obtain the *memory* function, in which the delay required is considerably larger than the duration of the input signal. These have been investigated mainly in connection with correlation of coded signals, and are considered in Chapter 10.

High-frequency Techniques. Generally, the maximum centre frequency obtainable is about 1.5 GHz, since this requires 0.5 μm line widths when single-electrode transducers are used [213]. Narrower line widths can be obtained by electron beam lithography [214], though this is not convenient for commercial devices. However, some special techniques enable higher frequencies to be obtained without requiring narrower line widths. A simple approach is to use a harmonic response of a transducer, for example, the third harmonic of a double-electrode transducer. If the

presence of the fundamental response is undesirable, it may be virtually eliminated in a two-transducer device by using transducers operated at different harmonics, as shown by Engan [215]. For example, the device may have an $S_e = 3$ transducer operated at the second harmonic and an $S_e = 4$ transducer operated at the third harmonic. In this case there is little overlap of the fundamental responses of the transducers. An additional advantage is that electrode interaction affects are minimised.

Generally, only the first few harmonics are useful for high-frequency operation, because for harmonic numbers greater than S_e the coupling efficiency of the transducer is found to be quite sensitive to the metallisation ratio a/p, which is difficult to control accurately for narrow electrodes. The sensitivity to a/p is due to rapid variations of the elemental charge density $\bar{\varrho}_f(\beta)$ with a/p, as shown in Figure 4.12. To overcome this difficulty, modified types of transducer have been proposed [216], using electrodes with different widths in each period. These transducers give harmonic responses less sensitive to errors in the electrode widths, though the coupling strength is rather weak.

Another method of obtaining higher centre frequencies is to use a wave with higher phase velocity. Appendix F discusses the use of bulk waves for this purpose, and another potential possibility is the use of aluminium nitride films, mentioned in Section 6.5.

7.2. MULTI-PHASE UNIDIRECTIONAL TRANSDUCERS

In Section 7.1.3 several methods for minimising triple-transit signals were discussed, and it was noted that unidirectional transducers offer both good triple-transit suppression and low losses. The multi-strip type of unidirectional transducer has been described in Section 5.4. In this section we describe the use of multi-phase unidirectional transducers. In contrast to the multi-strip type, the multi-phase method can be applied to transducers that are many wavelengths long, and also to transducers that are apodised. For these reasons, multi-phase transducers have been investigated extensively, and several types have been developed.

7.2.1. Transducer Types and Performance

The earliest type of multi-phase transducer was the *three-phase* type, introduced by Hartmann *et al.* [217] and shown in Figure 7.9(a). The electrodes are regular, and are connected sequentially to three bus-bars, with terminals A, B and C. Connections to one of the bus-bars must be made via insulating *cross-overs*, which are usually made with the aid of an insulating silicon oxide film, though air gaps have also been used [218]. The periodicity of the transducer is made equal to $\lambda_c = 2\pi v_0/\omega_c$, which is the surface-wave wavelength at the required centre frequency ω_c. Thus there are three electrodes per wavelength. The operation of the transducer is considered in detail later, but the essential features are readily appreciated if each electrode is regarded as a surface-wave source. For a surface wave of frequency ω_c travelling through the transducer, the phase angle corresponding to the electrode spacing is 120°. If voltages are applied to the three bus-bars, with the same amplitudes but with phases

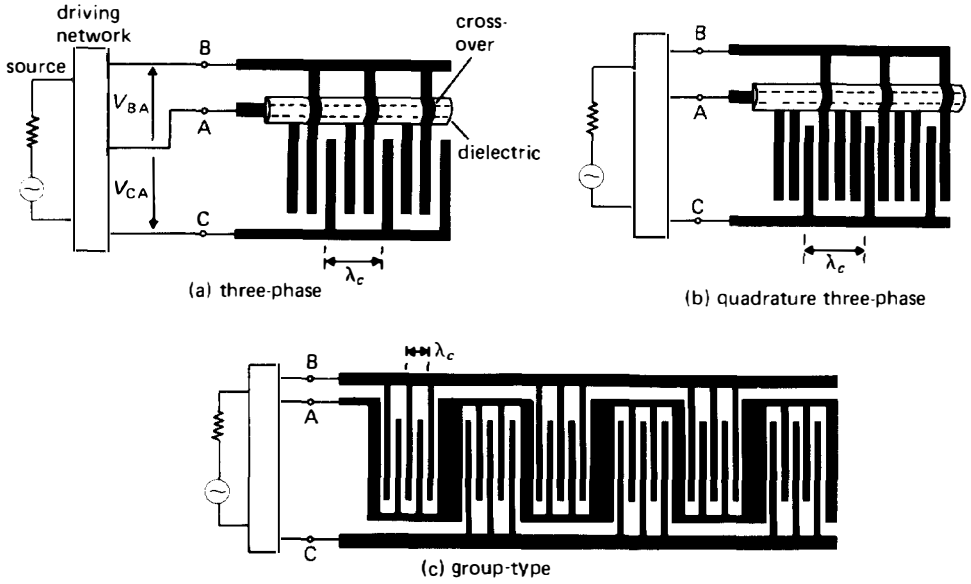

FIGURE 7.9. Multi-phase transducers.

incrementing by 120°, the waves generated in the "forward" direction have the same phase and thus reinforce. The waves launched in the "backward" direction, due to the three electrodes in any one period of the transducer, have relative phases of 0, 240° and 480°, and add vectorially to give a resultant of zero. Thus surface waves are generated only in one direction. It should be noted that only relative electrode voltages are significant, since a uniform voltage applied to all the electrodes gives no acoustic excitation. It is therefore sufficient to note the voltages relative to terminal A, say. The relative voltages, denoted V_{BA} and V_{CA}, have a phase difference of 60°.

The required voltages are produced by applying a source to a driving network comprising a few reactive components. This can be designed such that the transducer is matched, so that all of the power available from the source is converted into a surface wave propagating in one direction. In this case any surface wave incident on the transducer on the "forward" side is fully converted into electrical output power, with no acoustic reflection, as expected by reciprocity. However, a practical driving network can give the required phase relationship only at one frequency, so the transducer is unidirectional only at one frequency.

Figure 7.9(b) shows the *quadrature three-phase* transducer [219, 220] which operates in a very similar manner. There are now four electrodes per period and the period, as before, is equal to λ_c. For a propagating surface wave the electrode pitch corresponds to a phase change of 90°. Thus, to cancel the waves radiated in one direction the voltage on terminals B and C, relative to terminal A, should differ in phase by 90°. The structure is closely related to the earlier "hybrid-junction" transducer [221] in which the electrodes are connected sequentially to four bus-bars; this has been shown to be usable as a unidirectional transducer, though it does not

have appreciable advantages over the quadrature three-phase type. It should be noted that the transducers in Figure 7.9(a) and (b) give negligible electrode interaction effects, because the electrode pitch is not a multiple of $\lambda_c/2$.

The *group-type* transducer introduced by Yamanouchi *et al.* [222] is shown in Figure 7.9(c). The transducer consists of two interleaved sets of "groups", each group being essentially a conventional single-electrode transducer, though other types of structure may be used for the individual groups. The centre-frequency wavelength λ_c is equal to twice the electrode pitch in any one group. One set of groups is displaced relative to the other by $(N + \frac{1}{4})\lambda_c$, where N is some integer. Thus, unidirectional operation is obtained at frequency ω_c by driving the two sets of groups in phase quadrature. Since the centre-to-centre spacing of adjacent groups is several wavelengths, the appropriate phase relationship is obtained, to an adequate accuracy, only over a relatively narrow bandwidth. Thus this type of transducer is best suited for narrow-band devices. However, the transducer is particularly suitable for high-frequency devices since the electrode width required, for a given frequency, is larger than that of other multi-phase types.

Another advantage of the group-type transducer is that one of the three connections required can be provided by a meander line, as shown in Figure 7.9(c). This avoids the need for cross-overs and thus considerably simplifies the fabrication. However, care is needed to ensure that the resistance of the meander line is low enough. In some cases this resistance would cause unacceptable losses, but cross-overs can if necessary be introduced to overcome this problem, using an additional bus-bar at the side.

Malocha and Hunsinger [223] have introduced another group-type transducer, shown in Figure 7.10. This again has the advantage that a meander line can

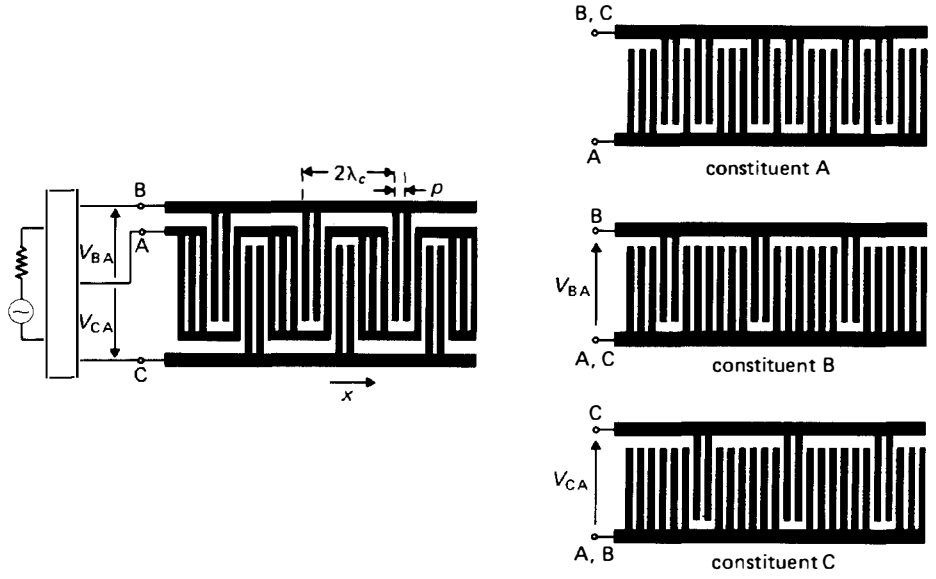

FIGURE 7.10. *Left*: Alternative group-type transducer. *Right*: Corresponding constituent transducers.

sometimes be used, simplifying the fabrication. The electrodes are regular here. The transducer period is of length $2\lambda_c$ and includes 8 electrodes, so that there are four electrodes per wavelength. The two-electrode groups connected to terminals B and C in Figure 7.10 have a relative displacement of $3\lambda_c/4$, so unidirectional operation is obtained at frequency ω_c if the relative voltages V_{BA} and V_{CA} are in phase quadrature with each other.

As for conventional two-terminal transducers, the structure of a multi-phase transducer may be modified in order to weight the response, for example, to produce a bandpass filter response with good sidelobe rejection. The commonest weighting technique is essentially the same as the apodisation technique applied to two-terminal transducers, that is, the electrode overlaps are varied along the length of the transducer. This method can be applied to all the transducer types mentioned above. Provided the electrode overlaps do not vary substantially in any one period, the transducer retains its unidirectional character, enabling low loss and good triple-transit suppression to be obtained. For narrow-band devices, withdrawal weighting is sometimes used.

Multi-phase transducers enable exceptionally low insertion losses to be obtained. For the best results, considerable care is taken to minimise losses due to imperfections such as electrode resistivity, surface-wave diffraction and resistance in the driving networks. In this way, Brown [224] demonstrated a 34 MHz three-phase device with only 0.6 dB insertion loss, and Yamanouchi *et al.* [225] obtained an insertion loss of 3 dB at 1.0 GHz using a modified form of group-type transducer. A variety of recent results show the performance achievable for bandpass filters using weighted transducers [226–228]. For example, a 650 MHz lithium niobate filter, using group-type transducers with apodisation, gave 7 dB insertion loss, 9 MHz bandwidth and 40 dB out-of-band rejection [227]. Withdrawal-weighted group-type transducers have been used effectively on *ST*, *X* quartz [228], giving for example, a 900 MHz filter with 5 MHz bandwidth, 8 dB insertion loss and 30 dB out-of-band rejection. In most of the devices the in-band ripple, due mainly to the triple-transit signal, was 0.2 dB peak-to-peak or less.

7.2.2. Analysis of Multi-phase Transducers

The analysis here is based on a charge superposition argument [229], which shows that the operation of a multi-phase transducer can be derived from the analysis of two-terminal transducers, given in Chapter 4. An alternative approach, obtained by generalising the crossed-field network model, is given by Farnell *et al.* [230]. For illustration we consider the group-type transducer, Figure 7.10, though the method is also applicable to the other types. It is convenient to assume that guard electrodes are used at each end of the transducer to eliminate end effects, though the analysis is approximately valid if the guards are absent.

(a) Launching Transducer. We first consider launching of surface waves. At the frequencies of interest the electrode pitch is not close to the half-wavelength, or to a multiple of this value, and therefore electrode interactions can be ignored. Thus the quasi-static analysis of Section 4.3, which allows for arbitrary electrode voltages, is

valid here. In particular, the potentials $\phi_s^{\pm}(x, \omega)$ of the surface waves generated in the $\pm x$ directions are, from equation (4.26),

$$\phi_s^{\pm}(x, \omega) = j\Gamma_s \bar{\sigma}_e(\mp k_0) \exp(\mp jk_0 x), \tag{7.24}$$

where $k_0 = \omega/v_0$ is the free-surface wavenumber at the frequency ω under consideration, and Γ_s is the piezoelectric coupling parameter given by equation (4.21). The function $\bar{\sigma}_e(\beta)$ is the Fourier transform of the electrostatic charge density of $\sigma_e(x)$. The charge superposition principle shows that this is given by equation (4.33), that is,

$$\sigma_e(x) = \sum_{n=1}^{N} V_n \varrho_{en}(x), \tag{7.25}$$

where N is the number of electrodes, V_n is the voltage on electrode n and $\varrho_{en}(x)$ is the electrostatic charge density produced when unit voltage is applied to electrode n with the other electrodes grounded.

In the present case there are only three distinct values of the electrode voltages, and since only relative voltages are significant it is sufficient to take terminal A to be at zero voltage, and to consider only the relative voltages V_{BA} and V_{CA} of terminals B and C. Each of the V_n in equation (7.25) can thus be equated with V_{BA}, V_{CA} or zero, and the charge density can therefore be written in the form

$$\sigma_e(x) = V_{BA}\varrho_e^b(x) + V_{CA}\varrho_e^c(x). \tag{7.26}$$

Here $\varrho_e^b(x)$ is the electrode charge density obtained when terminals A and C are grounded and unit voltage is applied to terminal B. Similarly, $\varrho_e^c(x)$ is the charge density when terminals A and B are grounded and unit voltage is applied to terminal C.

The method can be clarified by considering imaginary two-terminal transducers, called *constituent* transducers, shown on the right in Figure 7.10. Each of these is defined by imagining two terminals of the group-type transducer to be connected together. For constituent A terminals B and C are connected, for constituent B terminals A and C are connected, and for constituent C terminals A and B are connected. Thus, in equation (7.26), $\varrho_e^b(x)$ is equal to the electrostatic charge density on constituent B for unit applied voltage, and $\varrho_e^c(x)$ is the electrostatic charge density on constituent C for unit applied voltage. The constituent two-terminal transducers can be analysed by the methods of Chapter 4, and since the electrodes are regular here the methods of Section 4.5 can be applied.

From the geometries of constituents B and C, shown in Figure 7.10, it is clear that $\varrho_e^b(x)$ and $\varrho_e^c(x)$ are the same except for a displacement $3p$, where p is the electrode pitch. Thus $\varrho_e^c(x) = \varrho_e^b(x - 3p)$. The Fourier transforms of $\varrho_e^b(x)$ and $\varrho_e^c(x)$, denoted respectively by $\bar{\varrho}_e^b(\beta)$ and $\bar{\varrho}_e^c(\beta)$, are therefore related by

$$\bar{\varrho}_e^c(\beta) = \bar{\varrho}_e^b(\beta) \exp(-3j\beta p).$$

Taking the transform of equation (7.26), this enables $\bar{\sigma}_e(\beta)$, the transform of $\sigma_e(x)$, to be written in terms of $\bar{\varrho}_e^b(\beta)$. Substituting into equation (7.24), the potentials of the two surface waves launched by the transducer are

$$\phi_s^{\pm}(x, \omega) = j\Gamma_s \bar{\varrho}_e^b(\mp k_0)[V_{BA} + V_{CA} \exp(\pm 3jk_0 p)] \exp(\mp jk_0 x). \tag{7.27}$$

Now, at the centre frequency ω_c we have $\lambda_c = 4p$ and hence $k_0 p = \pi/2$, giving $\exp(\pm 3jk_0p) = \mp j$. Thus if $V_{CA} = jV_{BA}$, so that the voltages are in phase quadrature, we have $\phi_s^-(x, \omega) = 0$, so that the transducer radiates surface waves only in the $+x$ direction. Alternatively, if $V_{CA} = -jV_{BA}$ then $\phi_s^+(x, \omega) = 0$ and the transducer radiates only in the $-x$ direction. The surface-wave powers are given by equation (4.51).

The superposition principle can still be applied if the multi-phase transducer is apodised. In this case the constituent transducers are also apodised. Assuming the electrode voltages to be known, the waves generated by the multi-phase transducer can be found by summing the waves that would be produced by the constituents B and C.

(b) Equivalent Circuit. For a two-terminal transducer the admittance seen between the terminals is $Y_t(\omega) = G_a(\omega) + jB_a(\omega) + j\omega C_t$. Here we consider the admittances seen between the three terminals of a multi-phase transducer. These are needed in order to evaluate the electrode voltages V_{BA} and V_{CA} as functions of frequency, for a specified driving network, and to analyse reception of surface waves by the transducer.

Assuming that no acoustic waves are incident on the transducer, the terminal currents and voltages are taken to be related by the equivalent circuit of Figure 7.11(a), where admittances Y_{AB}, Y_{BC} and Y_{AC} are connected between the three terminals. This arrangement is sufficiently general to represent any linear passive three-terminal device. The terminals A, B and C correspond to the transducer terminals in Figure 7.10. The admittances are straightforwardly related to the admittances of the constituent transducers in Figure 7.10, denoted by Y_t^a, Y_t^b and Y_t^c for transducers A, B and C, respectively. If terminals B and C of the multi-phase transducer are connected together, the admittance between them and terminal A is, from Figure 7.11(a), $Y_{AB} + Y_{AC}$. This must be equal to the admittance Y_t^a of constituent transducer A. Similarly, by imagining terminals A and B or A and C to be connected, two further relations are found. These can be solved for the admittances of the multi-phase transducer, giving

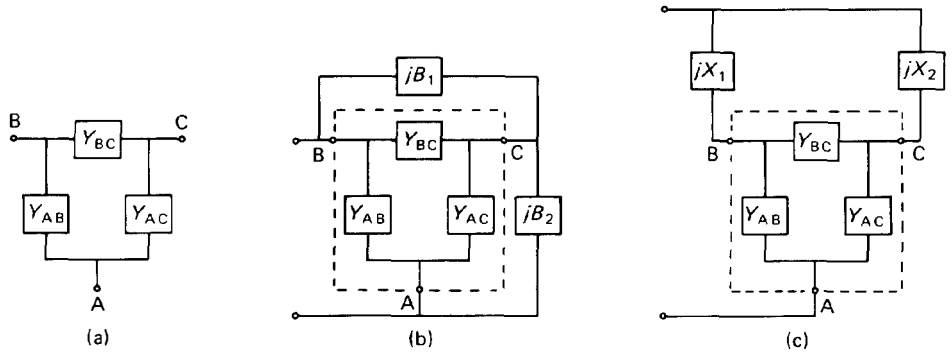

FIGURE 7.11. (a): Equivalent circuit of multi-phase transducer. (b), (c): Use of two components to provide required phase shift.

$$Y_{AB} = \tfrac{1}{2}(Y_t^a + Y_t^b - Y_t^c),$$
$$Y_{BC} = \tfrac{1}{2}(Y_t^b + Y_t^c - Y_t^a),$$
$$Y_{AC} = \tfrac{1}{2}(Y_t^a + Y_t^c - Y_t^b). \quad (7.28)$$

Since the admittances of the constituent transducers can be found by the methods of Chapter 4, these equations enable Y_{AB}, Y_{BC} and Y_{AC} to be evaluated. For the transducer of Figure 7.10 it can be seen that constituents B and C have essentially the same structure, so that $Y_t^b = Y_t^c$ and hence $Y_{AB} = Y_{AC}$. For the three-phase transducer of Figure 7.9(a), the three constituents are all the same except for a displacement, and hence $Y_{AB} = Y_{BC} = Y_{AC}$. In fact, the constituent transducers for this case are the same as the uniform $S_e = 3$ transducer, whose admittance has already been considered in Section 4.6.

(c) *Driving Networks.* Once the transducer admittances are known, either from the above analysis or by measurement, a driving network can be designed in order to provide the appropriate phase relationship between the terminal voltages, and to match the transducer to a source. The driving network usually consists of a few lumped reactive components. Two common methods of obtaining the required phase relationship are shown in Figures 7.11(b) and (c). In Figure 7.11(b), reactive elements with susceptances B_1 and B_2 are connected between terminals B and C and between terminals C and A, respectively. This method [224] is often used for the three-phase transducer of Figure 7.9(a). The susceptances B_1 and B_2 are to be chosen such that $V_{CA} = V_{BA} \exp(j\alpha)$ at the centre frequency ω_c, with $\alpha = \pi/3$ or $\pi/2$ for the transducers considered above. Writing $Y_{AB} = G_{AB} + jB_{AB}$, and corresponding expressions for Y_{BC} and Y_{AC}, analysis of the circuit of Figure 7.11(b) gives

$$B_1 = (G_{AC} + G_{BC}) \operatorname{cosec} \alpha - G_{BC} \cot \alpha - B_{BC}$$

and

$$B_2 = -(G_{AC} + 2G_{BC}) \tan \alpha/2 - B_{AC}. \quad (7.29)$$

Thus two reactive components are sufficient to obtain the required phase relationship, whatever the values of Y_{AB}, Y_{AC} and Y_{BC}. However since these admittances are frequency dependent, the phase difference between V_{CA} and V_{BA} will also be frequency dependent, so B_1 and B_2 are chosen to satisfy equation (7.29) at the centre frequency ω_c. The required value of B_1 is then obtained by using a capacitor, with $C = B_1/\omega_c$, or an inductor, with $L = -1/(\omega_c B_1)$, depending on the sign of B_1. The same remarks apply to B_2. A more general form of the solution is described by Farnell *et al.* [230].

In addition to providing the required phase relationship, the driving network must also match the transducer to a resistive source in order to minimise the loss and to suppress acoustic reflections. The impedance seen looking into the circuit of Figure 7.11(b) is usually complex, so some additional reactive elements are added to provide the matching. These can take the form of one of the two-component circuits of Figure 7.3.

An alternative circuit, using series reactances X_1 and X_2, is shown in Figure 7.11(c). This method [223] is often used for the group-type transducer of Figure 7.10, though

it is also applicable to other types of transducer. As before, the required reactances can be deduced from circuit analysis, applying the condition that $V_{CA} = V_{BA} \exp(j\alpha)$. In this case the expressions obtained are more complicated and it is convenient to simplify them by assuming that $Y_{AB} = Y_{AC}$, which is valid for all of the transducer types considered above. With this assumption, the required values of X_1 and X_2 are found to be given by

$$\begin{aligned} X_1 + X_2 &= 2[B_{AB} + 2B_{BC} + G_{AB}(G_{AB} + 2G_{BC})/B_{AB}]^{-1}, \\ X_1 - X_2 &= (\tan \alpha/2)(X_1 + X_2)(G_{AB} + 2G_{BC})/B_{AB}. \end{aligned} \tag{7.30}$$

As before, the required phase relationship can be obtained only at one frequency, and additional reactances are needed to match the transducer to a resistive source.

(d) Reception of Surface Waves. The above analysis can be used to deduce the conversion efficiency for a multi-phase transducer launching surface waves and, by reciprocity, this is equal to the conversion efficiency for the same transducer receiving surface waves. Thus for a device using two multi-phase transducers the insertion loss, as a function of frequency, can be obtained. However, it is necessary to consider the reception process explicitly if the acoustic reflection coefficient is to be obtained.

For a receiving transducer the equivalent circuit of Figure 7.11(a) must be modified to include sources due to the incident surface wave. The sources can be deduced by considering the terminal currents produced when the three terminals are shorted, as shown in Figure 7.12(a). For an incident wave with potential $\phi_i(x, \omega)$ uniform across the transducer aperture, we define I_B and I_C as the currents entering terminals B and C, respectively. Comparison with Figure 7.10 shows that I_B is equal to the short-circuit current produced by constituent transducer B when a wave with potential $\phi_i(x, \omega)$ is incident on it. Similarly, I_C is the current produced by constituent transducer C when the same wave is incident. The currents I_B and I_C can therefore be obtained by analysing the two-terminal constituent transducers, using the methods of Chapter 4; they are related to the electrostatic charge densities $\varrho_e^b(x)$ and $\varrho_e^c(x)$ by equation (4.67).

Figure 7.12(b) shows the equivalent circuit for this case, where the broken line encloses the transducer itself. To account for the currents produced in the external

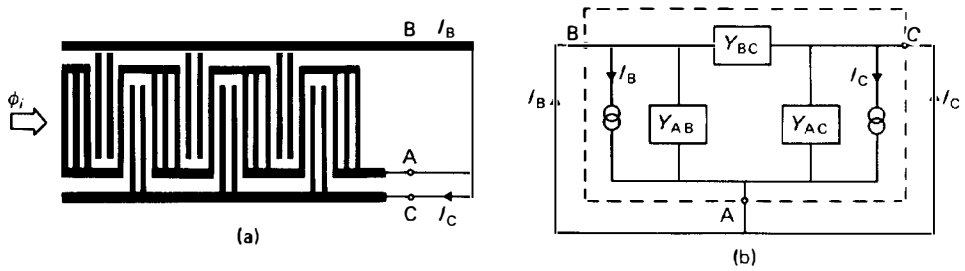

FIGURE 7.12. (a) Reception by shorted multi-phase transducer. (b) Equivalent circuit including current sources.

short circuit, a current generator I_B is added to the transducer equivalent circuit between terminals A and B, and a current generator I_C is added between terminals A and C.

The equivalent circuit of Figure 7.12(b), within the broken line, enables the performance of the receiving transducer to be calculated for any network connected to the terminals. Using conventional network analysis, the voltages V_{BA} and V_{CA} across the terminals can be found and the power delivered to the load can be calculated, thus giving the conversion loss. To calculate the reflected wave amplitude, it is first noted that electrode interactions can be assumed to be weak, so that the reflection coefficient is negligible if the transducer is shorted. The waves generated by the transducer can therefore be found by assuming terminal voltages V_{BA} and V_{CA}, and applying the analysis for a launching transducer as if the incident wave were absent. Thus the waves generated are given by equations (7.24) and (7.26), and the reflection coefficient can be obtained. For zero reflection coefficient it is found, as expected, that the transducer must be matched to the load, and the network must be such that it would provide the appropriate phases when launching surface waves.